

Near-field penetrating optical microscopy: a live cell nanoscale refractive index measurement technique for quantification of internal macromolecular density

Samantha Dale Strasser,¹ Gajendra Shekhawat,² Jeremy D. Rogers,¹ Vinayak P. Dravid,²
Allen Taflove,³ and Vadim Backman^{1,*}

¹Biomedical Engineering Department, Northwestern University, Evanston, Illinois 60208, USA

²Materials Science and Engineering Department, Northwestern University, Evanston, Illinois 60208, USA

³Electrical Engineering and Computer Science Department, Northwestern University, Evanston, Illinois 60208, USA

*Corresponding author: v-backman@northwestern.edu

Received October 6, 2011; revised December 13, 2011; accepted December 15, 2011;
posted December 15, 2011 (Doc. ID 154362); published February 8, 2012

Quantification of intracellular nanoscale macromolecular density distribution is a fundamental aspect to understanding cellular processes. We report a near-field penetrating optical microscopy (NPOM) technique to directly probe the internal nanoscale macromolecular density of biological cells through quantification of intracellular refractive index (RI). NPOM inserts a tapered optical fiber probe to successive depths into an illuminated sample. A 50 nm diameter probe tip collects signal that exhibits a linear relationship with the sample RI at a spatial resolution of approximately 50 nm for biologically relevant measurements, one order of magnitude finer than the Abbe diffraction limit. Live and fixed cell data illustrate the mechanical ability of a 50 nm probe to penetrate biological samples. © 2012 Optical Society of America

OCIS codes: 180.4243, 170.0180, 170.1530, 120.5710.

Numerous visible-light microscopy techniques exist to analyze intracellular structure based upon elastic interactions between light and cellular media. However, their spatial resolution is bounded by the Abbe diffraction limit and unable to resolve structures <200 nm [1]. A review of nanoscale technology indicates nonelastic techniques also present limitations. While fluorescence microscopy detects intracellular structures finer than the diffraction limit, it requires the addition of external agents to the cell, is incapable of analysis beyond tagged cellular species, and does not quantify density distributions [2]. Electron microscopy (EM) serves as a nanoscale imaging technique but does not image live cells and can require staining, preventing analysis of unaltered structure. While cryo-EM does not require staining it is limited to specific sample sizes and images frozen architecture [3].

The aim to understand biological processes at the nanoscale has been limited by a lack of suitable techniques. This knowledge is fundamental to multiple disciplines, e.g., disease progression, as nanoarchitectural changes can impact processes, e.g., gene transcription via higher-order chromatin structure [4] and protein folding within the cytoplasm via macromolecular crowding [5].

We developed NPOM to quantify nanoscale intracellular RI. RI is a linear function of macromolecular (proteins, DNA, RNA, and lipids) density via [6]

$$n = n_0 + \alpha\rho, \quad (1)$$

where n is RI, n_0 is RI of the medium (i.e., water, 1.33), α is the RI increment (~ 0.18 mL/g, experimentally determined and independent of chemical composition within measurement accuracy), and ρ is tissue solids by volume (g/mL) [6]. As this nanoscale molecular organization is linked to cellular processes, NPOM can provide unaltered cellular structure data for basic science research unattained by near-field techniques, e.g., near-field scan-

ning optical microscopy (NSOM) [7,8] and precision optical intracellular near-field imaging/spectroscopy technology [9].

NPOM penetrates a metal-coated fiber optic probe tapered to a 50 nm tip diameter into a sample in 20 nm increments at an illuminated lateral point, providing intracellular RI and macromolecular density data.

Electromagnetic field theory presents studies relevant to the ability of NPOM to quantify RI. Fischer [10] shows that it is possible to observe a monotonic linear relation between the coupled power and RI for an appropriate metallic film composition, thickness, illumination wavelength, and aperture dimension. NPOM provides this relation within the biologically relevant RI range.

NPOM data were collected using NSOM equipment (MultiView 1000, Nanonics, Inc.). A tapered optical fiber collects near-field optical data. While this system was originally designed for scanning surfaces, it is capable of incrementally moving the probe in the depth direction and can penetrate a probe into a sample. To permit collection of NPOM data, the scanning feature of the instrument is turned off and data collection time is set at or below 2 min (30 s for cell measurement allowing rapid data collection mitigating cell degradation).

We employed collection mode [11] with a metal-coated (Au/Cr or Ag/Cr) multimode optical fiber probe with a 50 nm tip diameter (Nanonics, Inc.), illuminated through an objective above the sample. We chose this modality as it collects signal in the near-field, providing measurements from the nanoscale volume at the probe tip [Fig. 1a].

The incident laser was an argon laser source having a total output power of the order of 10 mW. The wavelength was chosen to be either monochromatic (488 nm) or multiline. The latter explored effects of broadbanding the illumination. This source was aligned to a multimode optical fiber (Corning InfiniCor 600), which was mounted in place of an ocular on the optical microscope above the

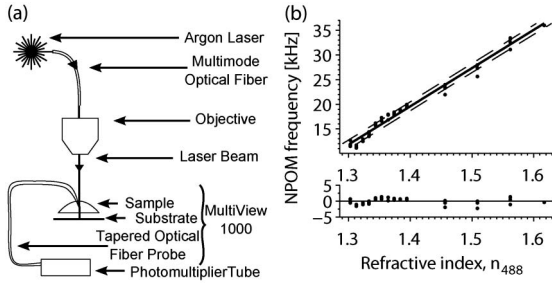


Fig. 1. (a) Schematic representation of NPOM. (b) Calibration curve relating RI to NPOM signal. Measurements are data points, the linear regression is solid black, and dashed lines represent RI uncertainty for a single measurement. Lower subplot displays residuals. The calibration equation is $y = mx + b$, where $m = 77 \pm 1.5$ and $b = -89 \pm 2.1$, and $R^2 = 0.98$ (confidence intervals represent the parameter's standard deviation).

MultiView 1000. This permitted the laser light to be focused through the objective and onto the sample. The probe tip was brought toward the sample surface and aligned over the illuminated spot allowing photon frequency detection by the photomultiplier tube, located on the nontapered probe end. The MultiView 1000 requires realignment for each new sample.

NPOM measurements collected while a probe was submerged in RI liquid standards (Cargille Laboratories, Inc.) within $n_D = 1.300$ to 1.600 ± 0.0002 provided the relationship between the NPOM signal and RI spanning the biological RI range. (n_D is the RI value at the sodium D -line; interpolation coefficients allowed extension to other wavelengths, i.e., 488 nm, where RI is noted as n_{488} .) Fourteen NPOM measurements, each a histogram of photon frequencies recorded by the detector, were collected per RI standard. Four measurements were performed per standard within $n_D = 1.3$ – 1.55 and one measurement for $n_D = 1.6$. The signals from $n_D = 1.55$ and 1.6 included some detector saturation, which was removed from the histogram before determining the calibration.

Figure 1b shows the NPOM signal for each measurement, quantified as the mean photon frequency f versus RI, n_{488} . These data constitute a calibration between NPOM signal and medium RI surrounding the probe tip. Linear regression analysis reveals a highly linear ($R^2 = 0.98$) relationship and a sensitivity, root mean square error (RMSE) and precision of $77f/\Delta n_{488}$, $0.87f$ and $0.88f$, respectively. Rearranging this calibration allows a measured f to be mapped to $n_{488} \pm \Delta n_{488}$ (Δn_{488} corresponds to the calculated standard deviation of n_{488}) [12]. While Δn_{488} varies along the calibration curve

Table 1. Interface Resolution Dependence on RI^a

n_D	2σ [nm]	RMSE [kHz]
1.300	140	0.33
1.370	50	0.40
1.380	40	0.45
1.450	<20	0.44
1.600	<20	0.12

^aRMSE is the goodness of fit for each RI; error on n_D is ± 0.0002 .

(smallest at the calibration centroid), its maximum is 0.01. Uncertainty intervals also account for alignment variations as each sample requires a new alignment. This calibration is unique to a probe, while linearity remains consistent.

Calibration data reveal a monotonic, linear relationship between the NPOM signal and RI within the biological range, $n_D = 1.3$ – 1.6 . This permits the NPOM signal to be uniquely mapped to the RI value surrounding the probe tip, a result consistent with Fisher's work [10].

We repeated calibration studies to directly compare the 488 nm and multiline laser modalities. The slope and intercept of each calibration were found to be within a standard deviation of the other modality's respective calibration parameters; thus, no statistically significant difference existed and broadbanding the incident laser does not significantly perturb the calibration.

NPOM's ability to resolve RI is determined by collecting data through an air and RI standard interface. Beginning in air, the probe was passed incrementally through the liquid in 20 nm steps, collecting data at each z position. Sigmoidal in shape, these data were fit to the sigmoidal function

$$g(z) = a + \frac{b}{2} \left[1 + \operatorname{erf} \left(\frac{z - \mu}{\sigma\sqrt{2}} \right) \right], \quad (2)$$

by minimizing the sum of square error in Microsoft Excel to determine the edge spread function (ESF), [Fig. 2a]. The ESF derivative is a Gaussian function (where a and b are constants, μ is the mean, and σ is the standard deviation) used to model a line spread function (LSF), shown in Fig. 2b. The spatial resolution defined by the Sparrow criterion—the distance between two LSFs such that their sum merges to form a single peak with no central minimum—was derived as 2σ for Gaussian functions [13].

Additional measurements indicate 2σ decreases as RI increases (Table 1).

NPOM was used to obtain the RI of live and fixed human buccal cells. Live cells were swabbed from the buccal mucosa and submerged in $1\times$ phosphate buffered saline (PBS) to ensure cells remained hydrated during measurements. This was pipetted onto a poly-L-lysine (Sigma Diagnostics) coated coverslip. Fixed cells were prepared on coverslips via dehydration in 70% ethanol.

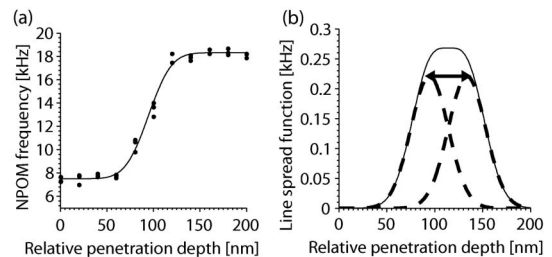


Fig. 2. (a) ESF measurements (data points) for RI liquid $n_D = 1.380 \pm 0.0002$ and fit (solid line) of the form of Eq. (2), where $a = 7.5$ kHz, $b = 10.8$ kHz, $\mu = 100$ nm, $\sigma = 20$ nm, RMSE = 0.45 kHz. (b) Dashed curves are the corresponding Gaussian LSFs. Separation between their central maxima is 2σ , 40 nm (double arrow) where their sum (solid line) forms a single peak.

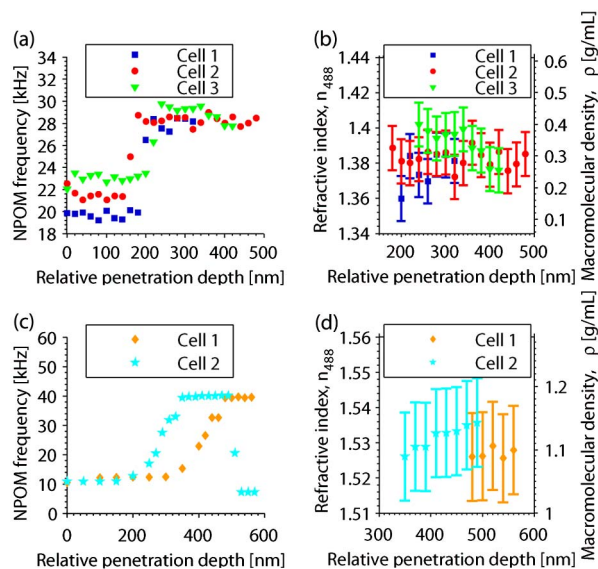


Fig. 3. (Color online) (a) NPOM data collected from the exterior into the interior of three live cells. (b) RI and ρ of the cellular interior in (a). (c) NPOM data collected from the exterior into the interior of two fixed cells. (d) RI and ρ of the cellular interior in (c). In (b) and (d) RI is obtained using $y = mx + b$, where $m = 78 \pm 2.4$ and $b = -79 \pm 3.5$ (confidence intervals are the standard deviation of the parameter) with $R^2 = 0.995$. RI data is related to ρ via Eq. (1).

Acknowledging cell drying may be a concern for live cells, we collected time series of the NPOM data at a fixed cellular location and determined there exists an ~ 25 min data collection window without significant cell drying.

NPOM measurements were collected from above and within the interior of three live, healthy buccal cells [Fig. 3a] and two fixed, healthy buccal cells [Fig. 3c]. These data were obtained using a 50 nm NPOM probe manually positioned at a point above the cell over the cytoplasm and penetrated into the cell in increments as small as 20 nm. Intracellular measurements correspond to the upper flat region of each dataset [Figs. 3a and c]. A linear calibration was used to calculate the intracellular RI [Figs. 3b and d].

Macromolecular density was calculated from RI via Eq. (1) [Figs. 3b and d]. These direct measurements provide intracellular RI and macromolecular density profiles previously unseen in the literature. As live cell measurements exceed the RI of PBS ($n \approx 1.33$) and are in agreement with macroscopic RI values previously reported in the literature, data show that the probe can penetrate a live cell and its interior membranes to collect internal nanoscale RI and macromolecular density [14].

NPOM measurements of fixed cells transition from air into the cellular interior indicating the NPOM probe is mechanically able to penetrate fixed cells. The RI values from the fixed cell interior [Fig. 3d] fall within the RI range of cellular components, such as a monolayer of double-stranded DNA ($n_{488} \approx 1.528$) [15], a lipid membrane ($n_{532} \approx 1.486\text{--}1.496$) [16], and dried/pure protein ($n \approx 1.53\text{--}1.6$) [6], validating NPOM's ability to measure the interior RI of fixed cells. The penetration depth into a fixed cell is limited. In Fig. 3c Cell 2, the signal drop at

160 nm into the cell likely results from cellular matter blocking the probe.

Cellular RI values [Figs. 3b and d] correspond to an interface resolution < 50 nm (Table 1). As the lateral resolution is comparable to the probe diameter, 50 nm, the spatial resolution for intracellular measurements is 50 nm.

NPOM directly measures intracellular RI and macromolecular density with a 50 nm spatial resolution for a 50 nm diameter probe, about one order of magnitude finer than the Abbe diffraction limit surpassing abilities of previous techniques [2,3,7–9,14,17–19]. Whether used for basic science research, as input data for computational models [20], or as a disease screening technique, NPOM has the potential to provide new opportunities for investigation of cellular biology at the nanoscale.

This work was supported by National Institutes of Health (NIH) grants R01CA128641 and R01EB003682, and National Science Foundation (NSF) grant CBET-0937987. S. D. Strasser was supported by the Chemistry of Life Processes Institute Undergraduate Research Grant (URG) and a Northwestern University (NU) Summer URG. V. P. Dravid was supported by the NCI-PSOC and NCI-CCNE program at NU. Data was collected at the NIFTI facility in the NUANCE Center.

References

1. E. Abbe, *Arch. Mikrosk. Anat.* **9**, 413 (1873).
2. S. W. Hell, *Science* **316**, 1153 (2007).
3. R. I. Koning and A. J. Koster, *Anat. Anz.* **191**, 427 (2009).
4. G. P. Delcuve, M. Rastegar, and J. R. Davie, *J. Cell. Physiol.* **219**, 243 (2009).
5. H. X. Zhou, G. Rivas, and A. P. Minton, *Annu. Rev. Biophys.* **37**, 375 (2008).
6. R. Barer and S. Joseph, *Q. J. Microsc. Sci.* **95**, 399 (1954).
7. L. Novotny and B. Hecht, *Principles of Nano-Optics* (Cambridge University, 2006).
8. F. H. Lei, G. Y. Shang, M. Troyon, M. Spajer, H. Morjani, J. F. Angiboust, and M. Manfait, *Appl. Phys. Lett.* **79**, 2489 (2001).
9. D. O'Connell and C. O'Connell-Rodwell, "Precision optical intracellular near field imaging/spectroscopy technology," U.S. patent 7,129,454 B2 (October 31, 2006).
10. U. C. Fischer, *J. Opt. Soc. Am. B* **3**, 1239 (1986).
11. E. Betzig, M. Isaacson, and A. Lewis, *Appl. Phys. Lett.* **51**, 2088 (1987).
12. D. C. Harris, *Quantitative Chemical Analysis*, 6th ed. (W. H. Freeman, 2002).
13. C. M. Sparrow, *Astrophys. J.* **44**, 76 (1916).
14. V. Backman and A. Wax, *Biomedical Applications of Light Scattering* (McGraw-Hill, 2010).
15. S. Elhadj, G. Singh, and R. F. Saraf, *Langmuir* **20**, 5539 (2004).
16. Y. L. Jin, J. Y. Chen, L. Xu, and P. N. Wang, *Phys. Med. Biol.* **51**, N371 (2006).
17. B. Rappaz, F. Charrière, C. Depeursinge, P. J. Magistretti, and P. Marquet, *Opt. Lett.* **33**, 744 (2008).
18. R. Drezek, M. Guillaud, T. Collier, I. Boiko, A. Malpica, C. Macaulay, M. Follen, and R. Richards-Kortum, *J. Biomed. Opt.* **8**, 7 (2003).
19. I. Itzkan, L. Qiu, H. Fang, M. M. Zaman, E. Vitkin, I. C. Ghiran, S. Salahuddin, M. Modell, C. Andersson, L. M. Kimerer, P. B. Cipolloni, K. H. Lim, S. D. Freedman, I. Bigio, B. P. Sachs, E. B. Hanlon, and L. T. Perelman, *Proc. Natl. Acad. Sci. USA* **104**, 17255 (2007).
20. A. Taflove and S. C. Hagness, *Computational Electrodynamics: The Finite-Difference Time-Domain Method*, 3rd ed. (Artech House, Norwood, Mass., 2005).